LANGMUIR

Article

Surface Coating Structure and its Interaction with Cytochrome *c* in EG Coated Nanoparticles Varies with Surface Curvature

Clyde A. Daly, Caley R Allen, Nikita D. Rozanov, Gene Chong, Eric S Melby, Thomas R. Kuech, Samuel E. Lohse, Catherine J. Murphy, Joel A. Pedersen, and Rigoberto Hernandez

Langmuir, **Just Accepted Manuscript** • Publication Date (Web): 17 Apr 2020

Surface Coating Structure and its Interaction with Cytochrome *c* in EG_6-Coated Nanoparticles Varies with Surface Curvature

Clyde A. Daly Jr.,[a] Caley Allen,[a] Nikita Rozanov,[a] Gene Chong,[a] Eric S. Melby,[b] Thomas R. Kuech,[b] Samuel E. Lohse,[c] Catherine J. Murphy,[c] Joel A. Pedersen,[b,d] and Rigoberto Hernandez[a,e,*]

[a] Department of Chemistry, Johns Hopkins University, Baltimore, MD 21218, United States
[b] Environmental Chemistry and Technology Program, University of Wisconsin – Madison, Wisconsin 53706, United States
[c] Department of Chemistry, University of Illinois Urbana-Champaign, Urbana, IL 61801, United States
[d] Departments of Soil Science, Chemistry, and Civil & Environmental Engineering, University of Wisconsin – Madison, Wisconsin 53706, United States
[e] Departments of Chemical & Biomolecular Engineering, and Materials Science and Engineering, Johns Hopkins University, Baltimore, MD 21218, United States

Abstract

The composition, orientation, and conformation of proteins in biomolecular coronas acquired by nanoparticles in biological media contribute to how they are identified by a cell. While numerous studies have investigated protein composition in biomolecular coronas, relatively little detail is known about how the nanoparticle surface influences the orientation and conformation of the proteins associated with them. We previously showed that the peripheral membrane protein cytochrome *c* adopts preferred poses relative to negatively charged MPA-AuNPs. Here, we employ molecular dynamics simulations and complementary experiments to establish that cytochrome *c* also assumes preferred poses upon association with nanoparticles functionalized with an *uncharged* ligand,

* Correspondence to r.hernandez@jhu.edu

specifically ω-(1-mercaptounde-11-cyl)hexa(ethylene glycol) (EG_6). We find that the display of the EG_6 ligands is sensitive to the curvature of the surface—and consequently, the effective diameter of the nearly spherical nanoparticle core—which in turn affects the preferred poses of cytochrome *c*.

Introduction

The interaction of gold nanoparticles (AuNPs) with cell membranes is fundamental to the characterization and prediction of more complex nanoparticle applications in drug delivery, photothermal therapies, diagnostics, and nanotoxicology.[1-5] In biological media (e.g., serum, lymph, cytosol, culture medium), a biomolecular corona often forms around nanoparticles as they interact with the surrounding milieu of biomolecules.[6-8] The characteristics of this corona are a function jointly of the biological medium in question and the properties of the nanoparticle itself.[9-11] The corona alters the properties and behavior of the nanoparticle in the biological system, including its interactions with cell membranes.[12-14] Protein coronas generally form in two steps with increased exposure of the nanoparticle to the biological system. Initially, high abundance, but perhaps low affinity, proteins associate with the nanoparticle. As exposure time increases, some of these high abundance proteins are displaced by lower abundance, but higher affinity proteins. The “end state” is a nanoparticle coated by a “corona” of proteins that may include both so-called “hard” and “soft” components. The hard and soft coronas display exchange kinetics with the medium that are slow and fast, respectively.[6, 15] The resulting “face” of the coronated nanoparticle depends not only on which proteins remain bound to the NP surface, but also on their preferred orientation and conformation on the

nanoparticle surface.[16] The pose —that is, the relative structure and orientation— of proteins near the nanoparticle surface, either as they approach or once attached, is generally sensitive to the chemistry and shape of the nanoparticle surface.[17-19] Here, we use the degree of interaction of nanoparticles to the surface of model membranes with and without an associated membrane protein as a proxy for the strength of the interaction between a protein and a nanoparticle, and we use simulations to investigate the characteristics of the binding.

Several groups have confirmed that properties of gold nanoparticles (e.g., size or functionalization) affect their function in biological systems.[20-26] A direct example of such function is binding to a bilayer. Melby, Lohse, *et al.*[27] used liquid chromatography-tandem mass spectrometry and quartz crystal microbalance with dissipation (QCM-D) monitoring to demonstrate that nanoparticles bearing distinct coatings bind to different sets of proteins and that the identity of the proteins rather than bulk properties such as zeta-potential influenced binding to bilayers. The nanoparticle surface chemistry and biological medium are important in determining the characteristics of the protein corona and impact the colloidal stability of nanoparticle suspensions.[9] Nanoparticle surface chemistry was demonstrated to affect the orientational preferences of α-synuclein on gold nanoparticles coated with citrate or myristyltrimethylammonium bromide using nuclear magnetic resonance (NMR) spectroscopy and molecular dynamics (MD) simulations.[28] In earlier work,[29] cytochrome *c* exhibited binding with preferred orientations to nanoparticles coated with an anionic ligand —namely, 3-mercaptopropionic acid (MPA). A lingering question remained as to whether this outcome requires the charge of the MPA-AuNP.

In the present work, we probed the interactions between supported lipid bilayers and nanoparticles functionalized with uncharged ligands as mediated by a peripheral membrane protein through a combination of large scale graphics processing unit (GPU)-accelerated classical MD simulations and QCM-D experiments[30] following protocols similar to those employed previously.[29, 31] These tools can reveal the sensitivity of surface structure and the pose of the protein—viz. cytochrome *c*—to the charge and curvature of the nanoparticle surface. In prior work, simulations focused on protein-membrane[31] and protein-nanoparticle interaction[29] without considering the effect of the radius of curvature of the nanoparticle. In contrast to our prior work with the anionic MPA ligand, here we use charge-neutral ω-(1-mercaptounde-11-cyl)hexa(ethylene glycol) (EG_6) as the ligand. We focused our simulations on probing the interaction between a protein and a nanoparticle with respect to variations in the radius of curvature of the nanoparticle. That is, we compare the behavior of the protein when interacting with nanoparticles of high curvature (i.e., small diameters: 2 nm, 4 nm, and 6 nm) to its behavior in response to a flat gold surface, corresponding to nanoparticles with very large (to infinite) diameters. Several groups have reported[32-35] that the behavior of longer and more flexible ligand molecules in nanoparticle coatings depends strongly on nanoparticle curvature, and we suspect that this in turn affects the formation of biocoronas. We perform a panel of simulations in which we vary the initial pose of the protein relative to different possible initial structures of the nanoparticle surface to identify possible relaxed (and preferred) equilibrium ensembles of poses. In these simulations, we maintain the density of the attached ligands at the NP surface constant so as to ensure that the local ordering close to the surface is comparable. The QCM-D experiments include all three components—viz., the

nanoparticle, the membrane binding protein, and the bilayer. In combination with our prior work, we are able to make comparisons to nanoparticles with different coatings and benchmark our simulations using the results of our experiments.

From simulation, we find that the strongly positively charged protein interacts much more weakly with a ligand-coated nanoparticle whose ligands are neutral (as in EG_6) than if they are negatively charged (as in MPA). The behavior of EG_6 on the NP surface is also highly affected by nanoparticle curvature. Our spherical nanoparticle systems exhibit a broad distribution of ligand arrangements, while the flat surface exhibits a uniform EG_6 structure. These curvature-induced differences in the ligand display lead directly to differences in the interactions between the protein and EG_6-coated nanomaterials. Increased curvature provides space for the ligands to adjust their structure to accommodate the protein. This allows the protein to draw nearer to the nanoparticle surface and to reside longer at those close distances. Unlike in the MPA case, the protein seems to have a fairly weak preference for specific orientations. The protein's interaction strength is correlated with curvature, likely because of the higher ligand flexibility and availability possessed by moderately curved nanoparticles.

Methods

Molecular Dynamics Simulations.

Simulation Parameters: All simulations of cytochrome *c* interacting with gold nanoparticles coated with ω-(1-mercaptounde-11-cyl)hexa(ethylene glycol) (EG_6) were run using the Nanoscale Molecular Dynamics program, version 2.13b1 (NAMD 2.13b1), unless otherwise noted.[36] The all-atom CHARMM36 force field was used to model all interactions.[37] The temperature was kept constant using a Langevin thermostat with a 5

ps^{-1} damping constant. In constant pressure simulations, pressure was maintained using a Langevin piston with a period of 1 ps and a decay rate of 50 fs was used. In all simulations, all bonds involving hydrogen were held fixed with SHAKE. Nonbonded interactions between atoms within three bonds of each other, or atoms further than 12 Å from each other were assumed to be zero and not included in the calculated forces except for long range electrostatics described by the Particle Mesh Ewald method with a grid spacing of 1.0 Å. A switching (or smoothing) function was applied to pairs of atoms between 8 and 12 Å. All simulations employed periodic boundary conditions and were propagated with a 2 fs timestep.

Simulation Setup: Twelve simulations were performed with EG_6 bound to a flat gold surface with dimensions 85 Å × 85 Å × 13 Å. Simulations using this structure are referred to as "flat surface" simulations. Eighteen simulations each were performed using 6 nm, 4 nm, or 2 nm diameter gold spheres with bound EG_6. Simulations using these structures are referred to as *"d* nm sphere" simulations, where *d* is the diameter. All systems were created by cutting the relevant structures out of a larger block of gold with an FCC crystal structure. EG_6 was added to the system using Packmol.[38] Ligands were placed such that their S atoms were within 3 Å of the gold surface, and oriented so that the atoms in each ligand were lined up at a surface density of 4 nm^{-2} as observed in experiment.[39] Visual Molecular Dynamics (VMD) was used to solvate each system in TIP3P water.[40-41]

The nanospheres were solvated within cubic boxes with 150 Å side lengths, and the flat surface was solvated within a box of dimensions 85 Å × 85 Å × 400 Å (with the additional length in the *z* direction occupied by water). These structures were equilibrated

using the Large-scale Atomic/Molecular Massively Parallel Simulator (LAMMPS) code,[42] to take advantage of functionality in LAMMPS unavailable in NAMD. These include the introduction of a 5.0 kcal mol^{-1} $Å^{-1}$ pulling force applied to sulfur atoms, directing them towards the gold surface, and the use of a Morse potential interaction (from Ghorai and Glotzer)[43] between the gold and sulfur atoms. After a short conjugate gradient minimization of the EG_6 and water atoms, *NPT* (1.01 bar, 300 K) dynamics were performed on the full system. The pressure was maintained using volume-scaling acting only on the long axis of the simulation box in the flat surface simulation and was maintained isotropically in the simulations of spherical nanoparticles. Once all of the sulfur had settled onto the gold and after additional equilibration, each sulfur atom was bonded to the nearest gold atom using parameters from the CHARMM36 force field. All water molecules from this step were removed prior to the addition of the protein.

Inclusion of the Protein: The peripheral membrane protein cytochrome *c* (structure 1AKK from the PDB) was used throughout this study.[44] A pre-equilibrated protein structure was inserted into the equilibrated nanoparticle system at one of six orientations as shown in Fig. 1, differing from each other by 90° rotations, such that the closest protein atom was 40 Å away from the flat gold surface and 25 Å from the nanosphere surfaces. These starting distances are similar to those used in a prior study of the interaction between this protein and gold nanospheres coated with MPA. The six cytochrome *c* orientations are chosen to lie along the principle axes of the protein so as to sample the space of possible orientations. In the simulations of nanospheres, each of these six protein orientations was inserted into three systems differing from each other by successive 90° rotations of the nanoparticle, producing 18 independent initial simulation

conditions for each diameter. In the flat surface simulations, the protein was placed above or below the surface in all six orientations, producing 12 independent initial simulation conditions. Since the protein is highly anisotropic and the nanoparticles are mostly isotropic (or have symmetry, in the flat case), we are able to use these initial conditions to obtain representative dynamics of a wide variety of possible protein-nanoparticle configurations. Each of these was then re-solvated in TIP3P water and ionized to an ionic strength of 0.01 M with NaCl using VMD.[40-41] In the flat case, the final box dimensions were again 85 Å × 85 Å × 400 Å; in the sphere cases the box dimensions were (d + 80 Å) × (d + 80 Å) × (d + 120 Å), where the protein and nanoparticle are centered along the longest axis and d is the diameter.

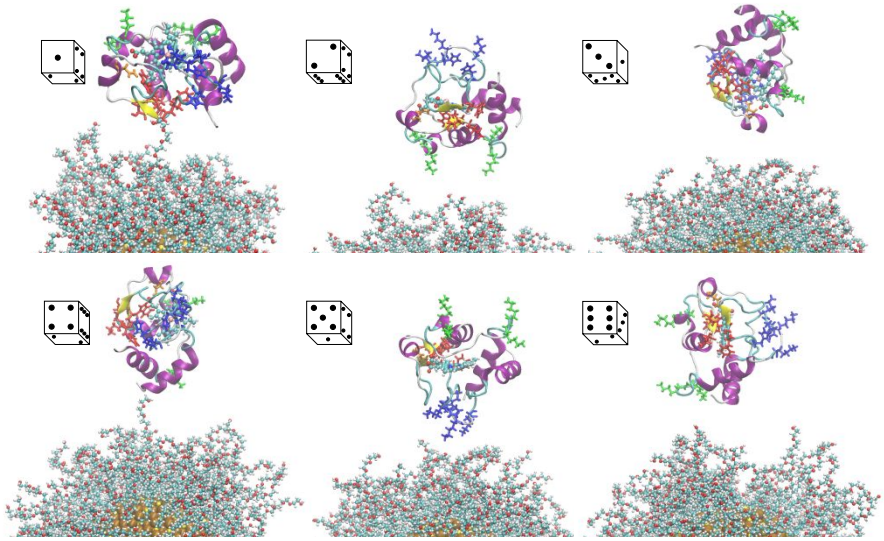

Figure 1. Locations of sites on protein and starting orientations of protein in simulation. The residues associated with each of 4 known binding sites of cytochrome *c* are highlighted here: A in green, of C in orange, of L in blue, and of N in red. Three simulations are run with the protein starting in each of these orientations relative to the spherical nanoparticles. For the flat surface simulations, two copies are run. In each case, the simulations with the same protein orientation differ by rotations of the ligated gold material.

Equilibration and Production Simulations: The combined protein-nanoparticle system was equilibrated in a multistep process. First, the system was subjected to 100,000 steps of conjugate gradient minimization. Then, the backbone atoms in the

protein, the iron and surrounding nitrogens of the heme group, and all gold atoms were held fixed while a 1 ns *NPT* (1 atm, 300 K) equilibration was performed. Volume scaling was permitted only along the longest axis of the periodic box in the flat surface simulations —which is also the direction perpendicular to the face of the surface—and was isotropic for the nanosphere simulations. The temperature was initialized at 5 K and was then allowed to rise smoothly to 300 K. The energy of the flat surface simulation configurations were subsequently minimized for 1,000 steps to remove bad contacts between different periodic copies of the gold slab. They were then reheated to 300 K in an *NVT* step. The constraints on both systems were progressively decreased over 600 ps, followed by 1 ns of equilibration with no constraints. Each simulation was run for an additional 100 ns in the *NVT* ensemble.

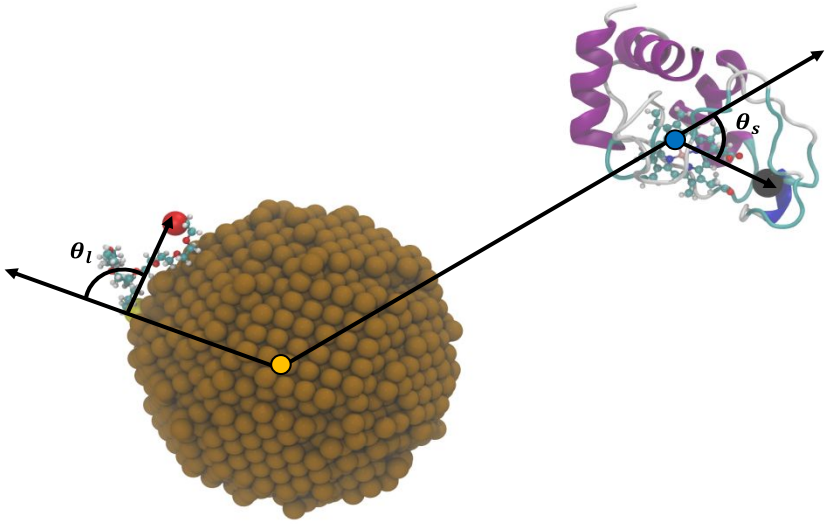

Figure 2. Pictorial description of the ligand angle (θ_l) on the left, and the site angle (θ_s) on the right. The orange circle represents the center of mass of the nanoparticle sans ligands, and the blue circle represents the center of mass of the protein. Water and most EG_6 ligands have been removed for clarity.

Numerical Measurements: During the simulations, the center of mass of four proposed binding sites A, C, L and N (highlighted in Fig. 1), the center of mass of the

entire protein, and the center of mass of the nanoparticle were tracked.[31, 45-47] To describe the interactions between the protein and the nanoparticle, and the behavior of the ligands, several angles were monitored. For the four protein sites, the angle between the vector from the protein center of mass to the site center of mass and the vector passing though both the nanoparticle and protein centers of mass was monitored. This is termed the "site angle" (θ_s). The angle between the vector from each S atom in each EG_6 ligand to the final O atom of the ligand, and the vector passing through both the center of mass of the nanoparticle and the S atom were also tracked. This angle, shown in Fig. 2, is termed the "ligand angle" (θ_l) and this definition is borrowed from Neidhart and Gezelter.[48] In addition, the distance of the final O atom of each ligand from the gold surface was monitored. In the flat surface simulations, the long axis (*z*) component of vectors related to the nanoparticle center of mass was used instead of the full vector in deference to the symmetry of the system.

The interaction energy between the nanoparticle and protein was calculated using VMD's NAMDenergy plugin.[40] Because of the wide variety of simulation conditions, diverse nanoparticle and protein configurations were sampled and are used to describe the protein-nanoparticle interaction. Data analysis was performed in Python using Jupyter notebooks and numpy.[49-50]

Experiments

Materials. All experimental materials were used as received, unless otherwise noted. Hydrogen tetrachloroaurate trihydrate ($HAuCl_4 \cdot 3H_2O$), sodium borohydride, glycerol (99% purity), and horse heart cytochrome *c* were purchased from Sigma Aldrich. Trisodium citrate dihydrate was obtained from Flinn Scientific. The EG_6-undecanethiol

ligand ($HS–(CH_2)_{11}–EG_6$) was synthesized following a published procedure.[51] We procured HEPES, NaCl, and $CaCl_2$ from Fisher Scientific. The phospholipids, 1,2-dioleoyl-*sn*-glycero-3-phosphocholine (DOPC), bovine liver α-phosphatidylinositol, and 1′,3′-bis[1,2-dioleoyl-*sn*-glycero-3-phospho]-*sn*-glycerol (TOCL) were purchased from Avanti Polar Lipids. All aqueous solutions were prepared in ultrapure water (>18 MΩ·cm). All solutions used were buffered to pH 7.4 with 0.01 M HEPES.

Nanoparticle synthesis and characterization. Gold nanoparticles (4-5 nm diameter) were prepared by borohydride reduction of $HAuCl_4$ in the presence of hydroxy-EG_6-undecanethiol as previously described.[52-54] The resulting EG_6-AuNP solutions were then purified by diafiltration.[54] Gold nanoparticle suspensions were diluted to 10 nM in 0.01 M NaCl solution and vortexed for 15 s, and their hydrodynamic diameter (d_h) and zeta-potential (ζ) were determined by dynamic light scattering laser and Doppler electrophoresis (Malvern Zetasizer Nano ZS), respectively. Reported d_h are number means of six measurements each consisting of 10 runs, while ζ values represent the average of six measurements each consisting of 20 runs.

Quartz crystal microbalance with dissipation monitoring. We employed QCM-D to monitor supported lipid bilayer formation, cytochrome *c* attachment to supported lipid bilayers, and the interaction of nanoparticles with supported phospholipid bilayers lacking or containing cytochrome *c*. Supported phospholipid bilayers were formed on SiO_2-coated QCM-D sensors from small unilamellar vesicles composed of pure DOPC, and DOPC containing 8.8% Liver PI, 4.4% TOCL, 8.8% TOCL, and 17.6% TOCL (percentages are mol%) via the vesicle fusion method as described previously.[31] For experiments employing cytochrome *c*, the protein was introduced to the flow cell as previously

described,[31] and cytochrome *c* electrostatically associated with anionic phospholipids. Either following bilayer formation and rinsing or protein attachment and rinsing, a solution of 10 nM EG_6-AuNPs in 0.01 M NaCl was flowed over the supported lipid bilayer lacking or containing the protein for 20 min to determine the extent to which the presence of cytochrome *c* alters EG_6-AuNP association with the supported phospholipid bilayer system. After the 20-min attachment period, nanoparticle-free solution was flowed for 20 min to assess the reversibility of nanoparticle binding.

QCM-D experiments employed a Q-Sense E4 system containing silica-coated sensors (QSX 303) mounted in temperature-controlled liquid flow cells (QFM 401; Biolin Scientific, Göteborg, Sweden). The instrument measures changes in both the resonant frequency and energy dissipation induced by the interaction of an analyte with the surface of the coated pieozoelectric quartz crystal. Changes in frequency (Δf) reflect changes in the acoustic mass coupled to the sensor surface (analyte mass and dynamically coupled solvent). Changes in the energy dissipation (ΔD) are related to the viscoelastic properties of laterally homogenous adlayers or the rigidity of particle-surface contact region for films of discrete nanoscale objects.[55] Experiments were conducted at 298 K.

Results

Simulations

Behavior of the Ligands. As reported in more detail below, the nature of the ligand strongly affects the nanoparticle's interactions with biological materials, and the nature of the nanoparticle affects the behavior of the ligand. We observed a stark difference, shown in Fig. 3, between the behavior of the EG_6 ligands across the four nanoparticle curvatures. The peak of these two-dimensional distributions with respect to the distance of the tail

end increases as curvature decreases indicating increasing extension of the ligand. EG_6 ligands on spherical gold nanoparticles exhibit a wide array of angles and effective lengths, including curled, wrapping, and extended ligand configurations as illustrated in Fig. 4. On the flat gold surface, however, the ligands almost always stand straight up with a mean length of about 29 Å. If the ligand density near the NP surface were varied, it would in principle be possible to counter some of the effects arising from the varying curvature. However, doing so might require unphysically high densities at the surface for the smallest NPs, or unreasonably spare coverage possibly leading to single chain behavior in the flatter cases. We have thus focused on keeping the density of the ligand attachments constant at the surface so as to avoid these confounding factors. In this way, we strictly examine the effect of curvature.

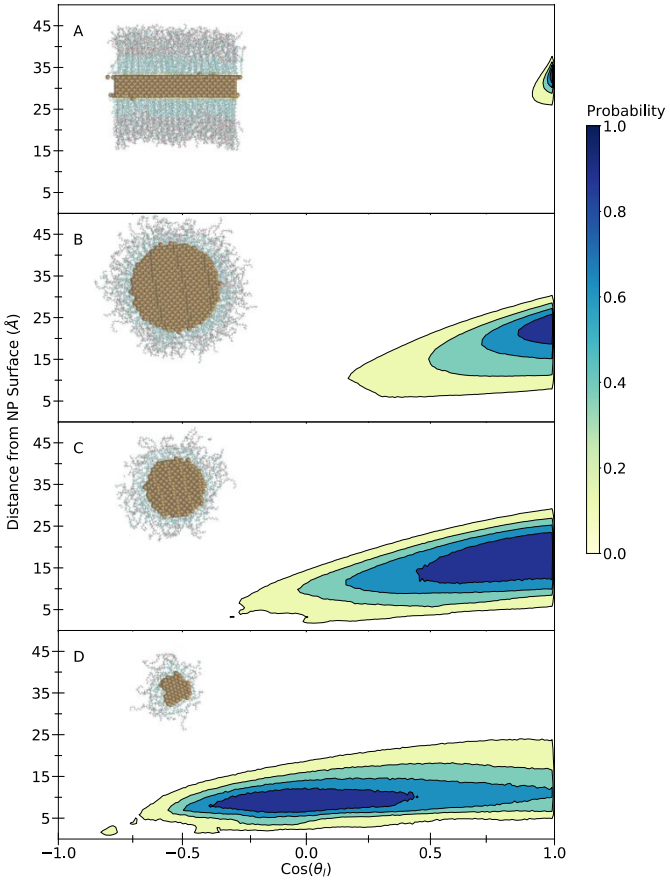

Figure 3. The probability distribution for finding the tail of an EG_6 ligand relative to the gold surface is shown for either a flat gold slab (A) or a spherical NP with a (B) 6 nm, (C) 4 nm, or (D) 2 nm gold core diameter. The reported distance is that of last O atom in the chain relative to the gold surface, and the angle θ_l is defined in Fig. 2. Representative structures of the nanostructures are also shown so as to provide a qualitative view in accord with the quantitative spatial probability distributions.

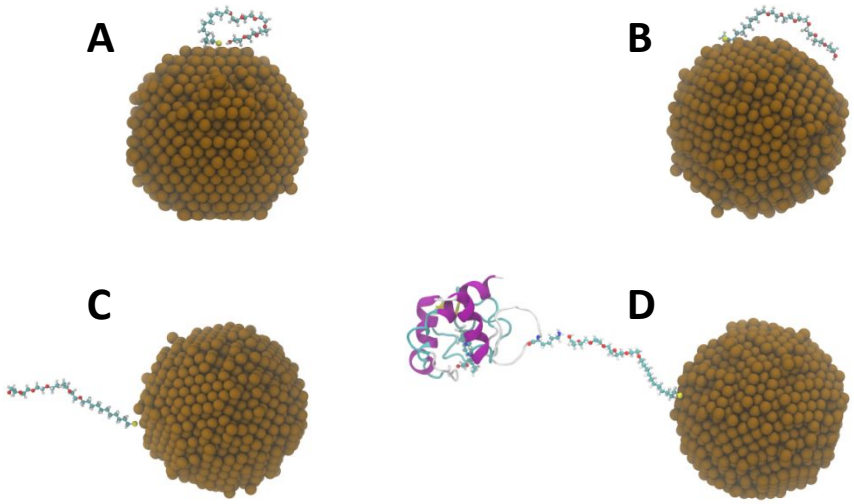

Figure 4. Representative snapshots of the behavior of EG_6 ligands during the sphere simulations. Configurations where the ligand is (A) curled, (B) wrapping, and (C) extended are shown. Also shown (D) is an extended ligand hydrogen bonding with a distant protein. Water and most EG_6 ligands have been removed for clarity.

The outcomes among the nanospheres is also diverse. The ligands around the 6 nm and 4 nm spheres have roughly similar distributions, with the smaller particle allowing somewhat more angular freedom. However, like in the flat surface, the ligands prefer to stand straight up over other configurations, maximizing the hydrophilic ligand headgroup exposure to water. The ligands on the 2 nm sphere are the only population without a preference to stand straight up, instead preferring to wrap in a wide range centered about halfway around the nanoparticle. This occurs because the hydrophobic portions of the ligands tend to lie flat on the gold surface, while the hydrophilic groups occupy a variety of configurations in the solvent. Combined, this favors ligand configurations with moderate ligand wrapping. These findings agree with prior NMR and MD results work which showed

that long chain ligands pack less randomly as nanoparticle curvature is decreased.[56-57] Based on these results, we categorize these structures into three regimes of curvature: low (flat), moderate (4 nm and 6 nm nanospheres), and high (2 nm nanosphere).

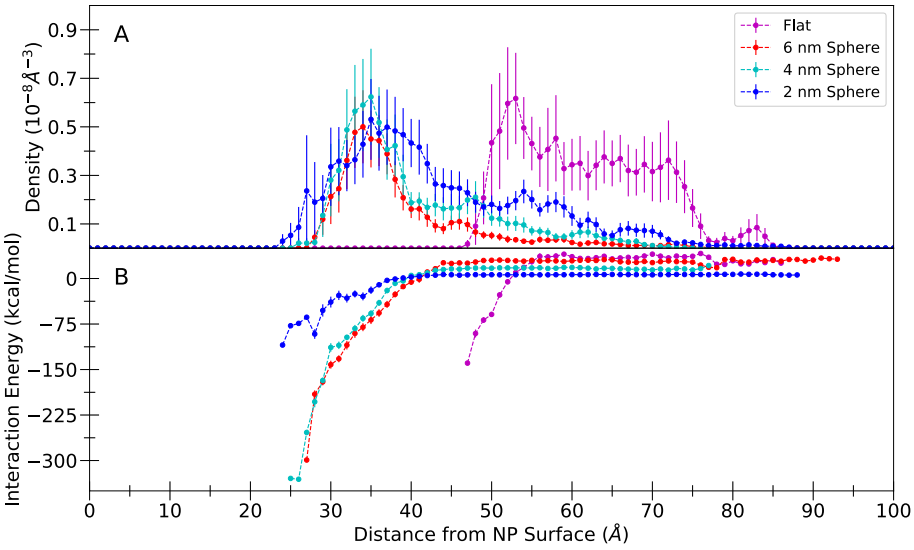

Figure 5. (A) Protein densities and (B) average interaction energy plotted as a function of protein-nanoparticle distance during the final 80 ns of each simulation. Error bars are standard errors across simulations where the given protein-nanoparticle distance was observed.

Interaction Energy of the Protein with the Nanoparticle. The average interaction energy (van der Waals plus electrostatic) between the protein and the nanoparticle was calculated for all simulation snapshots and is plotted against the distance of the protein from the nanoparticle surface in Fig. 5, along with the density of cytochrome *c* observed at various distances from the nanoparticle surface for the final 80 ns of each simulation. The first 20 ns were excluded to avoid the initial protein placement biasing the averages. The interaction energy is the sum over all pairwise interactions between atoms in the nanoparticle and atoms in the protein,

$$V_I(r_{PN}) = \left\langle \sum_i^N \sum_j^M \frac{q_i q_j}{r_{ij}} + \epsilon_{ij}\left[\left(\frac{R_{ij}}{r_{ij}}\right)^{12} - \left(\frac{R_{ij}}{r_{ij}}\right)^{6}\right] \right\rangle$$

(1)

where *N* is the number of atoms in the nanoparticle and *M* is the number of atoms in the protein, and *i* and *j* index each set of atoms, respectively. q_k is the charge of atom *q*, and R_{ko} and ϵ_{ko} are the Lennard-Jones parameters arrived at through the appropriate Lorentz-Berthelot mixing rules for the interaction between atoms *k* and *o*. Finally, r_{ko} is the distance between atoms *k* and *o*. The average is taken over snapshots with protein-nanoparticle distances between r_{PN} and $r_{PN}+1$ Å. Ewald summation was used for long range electrostatics, and the cutoff for short range electrostatics and van der Waals interactions was 12 Å with a smoothing function between 8 Å and 12 Å. The energies of distances that were never observed in simulation are not plotted. The protein comes much closer to the nanosphere surfaces than the flat surface, mainly as a result of the behavior of the EG_6 ligands. The closest the protein center of mass approaches the nanoparticle surface is approximately 26 Å in the nanosphere simulations and 47 Å in the flat surface simulations. In the flat surface simulations, the EG_6 molecules form a unified surface that the protein is unable to penetrate, although contact is sometimes made. In contrast, the EG_6 molecules around the nanospheres are often not fully extended, resulting in an overlap between the distance distributions of the protein and EG_6 molecules.

The protein-nanoparticle interaction energy profiles differ dramatically among the nanoparticle geometries examined, as shown in Fig. 5B. The minimum of the interaction energy for the 4 nm and 6 nm spherical nanoparticles is much lower than that for the flat surface or 2 nm nanosphere. The resulting energy differences across these nanospheres with varying diameter likely results from the different conformational flexibility of the ligands. The hydrophilic portions of the mobile ligands on the 4 nm and 6 nm nanospheres

are more easily able to reorganize so as to accommodate the protein structure than the stiff ligands on the flat surface. While the ligands on the 2 nm sphere are quite flexible, they are often wrapped around the nanoparticle and are thus not available to stabilize the protein.

Even in the most favorable cases, the protein and nanoparticles rarely make sustained contact. The protein is considered to be in contact with the nanoparticle if any heavy (*i.e.*, non-hydrogen) atom in the protein is within 3 Å of any heavy atom in the nanoparticle, including ligands. For the flat surface simulations, this criterion was fulfilled for over half of the simulation time in only 2 out of 12 simulations. This value is 8 out of 18, 6 out of 18, and 0 out of 18 for the 6 nm, 4 nm, and 2 nm nanosphere simulations, respectively. The radius of curvature and contact time are generally correlated for the nanospheres. The flat surface breaks this trend, displaying what would seem to be anomalously low interaction for its low curvature. We attribute these effects to the behavior of the ligands—the flat surface has the most distinct and inflexible ligands. These observed contact times should be contrasted with the behavior of the protein near the MPA-coated gold nanoparticles of our prior studies[31] where the protein generally engaged in sustained contact with the nanoparticle. This indicates a much weaker interaction between the EG_6 coated nanoparticles and cytochrome *c* than between the same protein and MPA-coated nanoparticles.

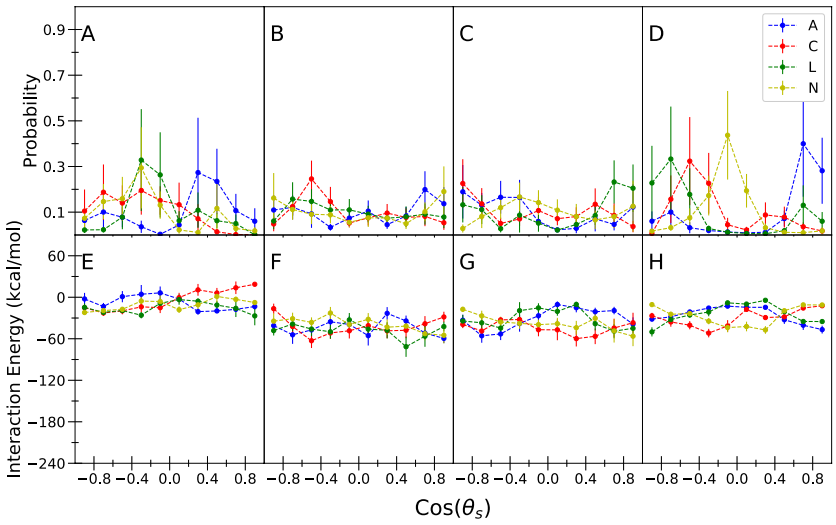

Figure 6. Orientation probabilities (A-D) and interaction energies (E-F) as a function of site angle for cytochrome *c* when interacting with a flat gold slab (A and E) or a spherical NP with a 6 nm (B and F), 4 nm (C and G), or 2 nm (D and H) core diameter coated with EG_6. Snapshots are only included if the protein is in contact with the nanoparticle. Error bars are standard errors across simulations where a given configuration was observed. The site angle, θ_s, is defined in Fig. 2.

Orientation of the Protein**.** Figure 6 shows the interaction energy of the protein at particular site angles when interacting with the nanoparticle. The site angle plotted in the horizontal axis of the figure is described in Fig. 2. Protein configurations were binned only when the protein and nanoparticle were in contact. As noted above, the protein was considered to be in contact with the nanoparticle if any heavy (*i.e.,* non-hydrogen) atom in the protein was within 3 Å of any heavy atom in the nanoparticle, including ligands. In the convention adopted in this work, $\cos(\theta_s) = -1$ when the center of mass of the site points directly towards the nanoparticle relative to the protein's center of mass, and $\cos(\theta_s) = 1$ when it points exactly away from the nanoparticle. Distributions for the flat surface, 6 nm sphere, 4 nm sphere, and 2 nm sphere are shown from left to right.

Near the flat slab, the protein prefers to have site A pointed slightly away from, site C and N pointed generally towards, and site L slightly towards to the surface. When in

contact with the 6 nm nanosphere, the preferences are changed. Site C prefers to point slightly towards the surface while sites A and N prefer to point towards or away from it. Site L seems to have no strong preferences. The 4 nm nanoparticle again has different preferences for protein orientation, promoting configurations where sites A, C, and L are pointed towards its surface while site N is orthogonally oriented. Sites L and C also often point away from the nanoparticle. Around the 2 nm nanosphere, the protein prefers to point sites L and C towards the surface, and site A away from it. Site N prefers to point perpendicular to the surface.

The strength of these preferences as indicated by the interaction energy is generally the same in all cases. Additionally, these energetic preferences are reflected in the orientational probabilities. However, it should be noted that the orientational probabilities themselves are highly uncertain as indicated by the large error bars. Further research is needed to produce more confident orientational predictions.

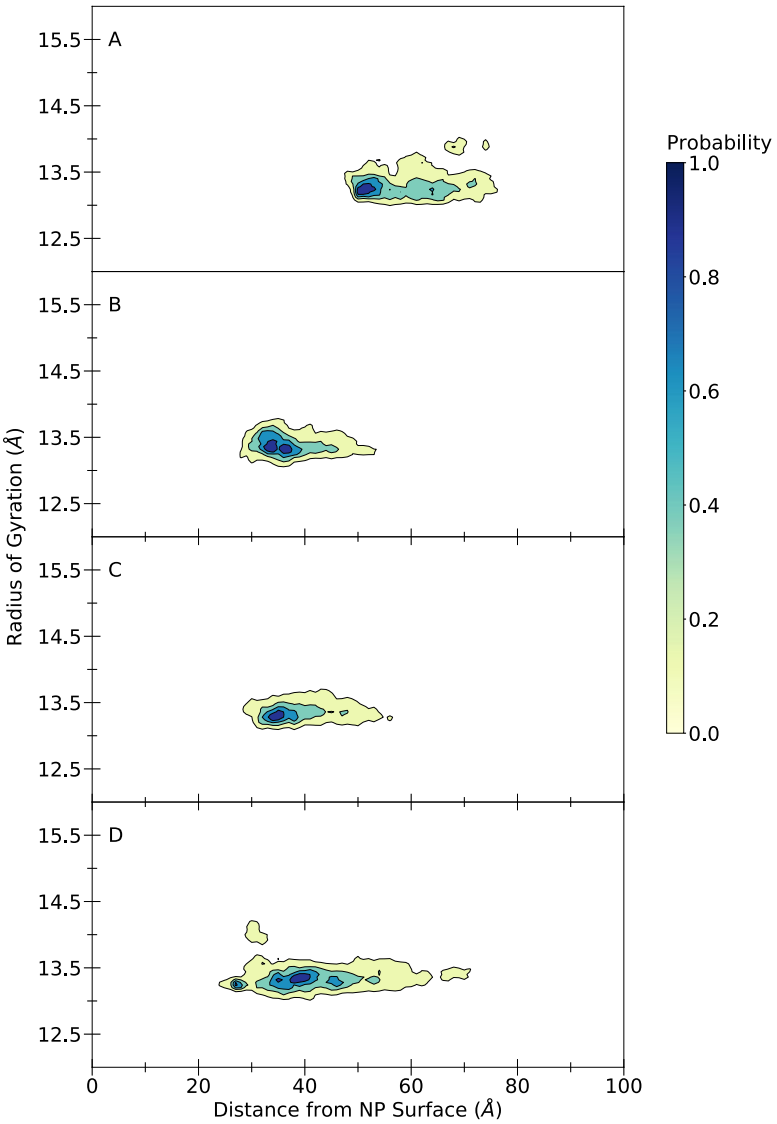

Figure 7: Radius of gyration for cytochrome *c* in solution when it is in proximity to a gold flat slab (A) or a spherical gold NP with a 6 nm (B), 4 nm (C), or 2 nm (D) core diameter coated with EG_6 as a function of distance from the gold surface.

Protein Structure**.** Cytochrome *c* is only moderately likely to interact with the EG_6 coated nanoparticles. This may indicate that it must become restructured in some way to do so. To investigate this hypothesis, we calculated the radius of gyration (r_g) of the protein across all trajectories and plotted r_g as a function of the distance from the nanoparticle surface in Fig. 7. Because of the differing ligand behavior, the protein is able

to approach the spherical nanoparticle surfaces more closely than what is seen in the flat case, as was also observed in Figs. 3 and 5. The protein explores the widest range of distances in the 2 nm nanosphere case because the interaction between the protein and nanoparticle is weaker as the surface becomes flatter, The majority of the sampled population shows the protein a moderate distance from the ligand surface with a radius of gyration near the native value of 13.6 Å.[58] Thus, there is no curvature-related effect on the internal structure of the protein for this neutral ligand.

Experiments

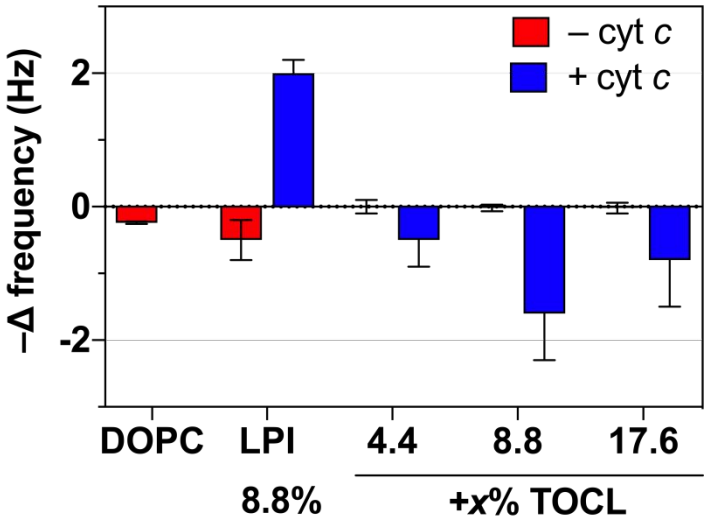

Figure 8: Attachment of EG_6-AuNPs to supported lipid bilayers composed of DOPC and liver PI (LPI) or cardiolipin (TOCL) lacking or containing cytochrome *c*. Error bars represent one standard deviation of triplicate measurements.

Nanoparticle Interaction with cytochrome c-containing model membranes. The gold nanoparticle cores were 4.1 ± 1.1 nm in diameter as determined by transmission electron microscopy. The hydrodynamic diameter and zeta potential (ζ) of the EG_6-AuNPs in 0.01 M NaCl buffered to pH 7.4 with 0.01 M HEPES were 7 ± 3 nm (see the Supporting Information for the distribution in hydrodynamic diameter) and −11 ± 3 mV, respectively.

These data indicate that the EG_6-AuNPs were likely not aggregated under the solution conditions employed. Our experimental observation of a moderately negative zeta potential for PEG-coated nanoparticles is consistent with literature precendent.[59-60] It presumably arises either from residual anions on the surface after the ligation with the neutral EG_6 , or a nonuniform penetration of ions inside and outside the coating.

We investigated the interaction between EG_6-AuNPs and each of the phospholipid bilayers discussed above (viz. DOPC, and DOPC containing 8.8% Liver PI, 4.4% TOCL, 8.8% TOCL, or 17.6% TOCL) in the absence and presence of cytochrome *c* by QCM-D. We observed negligible attachment of EG_6-AuNP to supported DOPC bilayers lacking or incorporating Liver PI or TOCL in the absence of cytochrome *c* (Fig. 8). Incorporation of cytochrome *c* into DOPC membranes containing 8.8% Liver PI promoted EG_6-AuNP attachment. We did not observe attachment to the DOPC bilayers containing TOCL bilayers with bound cytochrome *c*. This contrasts with the results obtained for the MPA-AuNPs, where we observed increasing attachment to those bilayers incorporating more anionic phospholipid,[31] which was most likely attributable to the increasing amount of membrane bound cytochrome *c*. These results may reflect a cytochrome *c* orientation-specific effect, since the orientation of the protein differs on bilayers containing Liver PI vs. TOCL. The orientation specificity could arise from one of the four binding sites of cytochrome *c* summarized above, and for which at least three interact non-negligibly with phospholipids: the electrostatic A- and L- sites and the hydrophobic C-site.[61-62]

Discussion

The present experimental and simulation results show an interaction between membranes with adsorbed cytochrome *c* and EG_6-coated spherical gold nanoparticles

that is fickle and depends strongly on the characteristics of the model membrane and nanoparticle surface. The simulations reveal low binding affinities between the nanoparticle and protein. The protein maintains contact with the EG_6 coated flat gold surface for 20 $\pm$ 8 % of the simulation time, with the EG_6 coated 6 nm gold nanosphere for 42 $\pm$ 7 % of the simulation time, with the 4 nm gold nanosphere for 27 $\pm$ 6 % of the simulation time, and with the 2 nm gold nanosphere for 7 $\pm$ 3 % of the simulation time. Additionally, even when EG_6 coated nanoparticles are absorbed to cytochrome *c* coated bilayers, the mass absorbed is relatively small. This is in stark contrast to prior experiments and simulations of MPA-coated gold nanoparticles interacting with the same types of biomolecules. In that case, the nanoparticles strongly bind to cytochrome *c* and to membranes with cytochrome *c* present (given that the cytochrome *c* itself binds to the bilayer).[29, 31] In all 6 configurations initialized there, cytochrome *c* came into contact with the MPA coated nanoparticle within about the same timescale as observed in this work with respect to the EG_6 coated nanoparticles, and retained contact for the duration of the simulations.[29]

Varied nanoparticle behavior is observed in experiment with respect to membrane formulation even when cytochrome *c* is adsorbed. This may be because incorporation of anionic lipids differing in headgroup (phosphate substituted with inositol for LPI vs. two phosphates for TOCL) into the model membranes promote dissimilar protein orientations, leaving distinct regions of the protein available to the nanoparticle for binding. In previous work, cytochrome *c* was found to promote the binding of nanoparticles with anionic ligands to model membranes containing TOCL in part by binding to the membrane surface in configurations that left sites A and L available to the nanoparticle for further

binding. However, only site A remains available when the bilayer contains Liver PI.[31] We have also found that cytochrome *c* is highly likely to interact with an MPA ligand-coated gold nanoparticle, particularly at sites L and A and many individual lysine residues.[29] In the experiments reported in this work, cytochrome *c* facilitated EG_6-coated nanoparticle binding to DOPC bilayers containing Liver PI, but not those containing various amounts of TOCL. In the current experiments, we observe nanoparticle attachment only in the Liver PI case. It is unclear if the current experimental results reveal binding site orientation because such length scales are not probed directly. However, in the light of our prior simulations, this experimental result implies that the nanoparticle preferentially binds to site A in the protein. However, if the nanoparticle binds to site A, then it seems it should also bind to the TOCL-containing membrane when cytochrome *c* is attached and presumably also exposing site A. This behavior is not observed in experiment. It may be that in the TOCL case, an insufficient population of protein sites A is available for the nanoparticle to bind with for the mass to be detected. We note that the simulations being used to interpret the Liver PI experiments were performed using bilayers made of a 9:1 mixture of DOPC and 18:0-20:4-phosphoinositol (SAPI). SAPI is the second most common species in Liver PI; the other species present may also have an effect on the protein orientation. The current simulations reveal that the moderate curvature nanoparticles (most similar to those used in experiment) can favorably bind with site A, showing agreement with the experimental results when interpreted through the lens of our prior simulations. However, it seems likely that that there is a nanoparticle-protein-bilayer effect that cannot be captured in models using only two of these elements.

Conclusions

In this work, we have characterized the behavior of a positively charged protein, cytochrome *c* and gold nanoparticles using molecular dynamics simulations and quartz crystal microbalance experiments. The gold nanoparticle systems differ in terms of their curvature and are coated with an uncharged ligand, $EG_{6,}$ in contrast to earlier work using negatively charged MPA ligands. We find that due to large differences in the ligand behavior, the protein interacts with the moderately curved spherical nanoparticles more strongly than the flat surface or a highly curved 2 nm nanosphere. However, all of the EG_6-coated nanoparticles, regardless of diameters, that we interrogated interact with the protein weakly in comparison to the previously studied anionic MPA-coated gold nanoparticles, in agreement with the experiments presented here and elsewhere. The protein shows some weak orientational preferences in each case and is largely not induced towards restructuring by interaction with the nanoparticle.

Supporting Information

The Supporting Information is available free of charge at TK. It provides Figure S1 showing the experimentally obtained distribution of hydrodynamic diameters for the EG6-AuNPs used in this work.

Acknowledgements

This work was supported by National Science Foundation under the NSF Center for Sustainable Nanotechnology (CSN), CHE-1503408. The CSN is part of the NSF Centers for Chemical Innovation Program. Computing resources were provided in part by the National Science Foundation through the Extreme Science and Engineering Discovery Environment (XSEDE) —which is supported by NSF grant number ACI-1548562— under

grant number CTS090079 and by the Maryland Advanced Research Computing Center (MARCC).

References

1. Abadeer, N. S.; Murphy, C. J. Recent Progress in Cancer Thermal Therapy Using Gold Nanoparticles. *J. Phys. Chem. C* **2016,** *120*, 4691-4716.
2. Zhou, W.; Gao, X.; Liu, D.; Chen, X. Gold Nanoparticles for in Vitro Diagnostics. *Chem. Rev.* **2015,** *115*, 10575-10636.
3. Torii, Y.; Sugimura, N.; Mitomo, H.; Niikura, K.; Ijiro, K. Ph-Responsive Coassembly of Oligo(Ethylene Glycol)-Coated Gold Nanoparticles with External Anionic Polymers Via Hydrogen Bonding. *Langmuir* **2017,** *33*, 5537-5544.
4. Buchman, J. T.; Hudson-Smith, N. V.; Landy, K. M.; Haynes, C. L. Understanding Nanoparticle Toxicity Mechanisms to Inform Redesign Strategies to Reduce Environmental Impact. *Acc. Chem. Res.* **2019,** *52*, 1632-1642.
5. Murphy, C. J.; Vartanian, A. M.; Geiger, F. M.; Hamers, R. J.; Pedersen, J.; Cui, Q.; Haynes, C. L.; Carlson, E. E.; Hernandez, R.; Klaper, R. D., et al. Biological Responses to Engineered Nanomaterials: Needs for the Next Decade. *ACS Cent. Sci.* **2015,** *1*, 117-123.
6. Milani, S.; Baldelli Bombelli, F.; Pitek, A. S.; Dawson, K. A.; Rädler, J. Reversible Versus Irreversible Binding of Transferrin to Polystyrene Nanoparticles: Soft and Hard Corona. *ACS Nano* **2012,** *6*, 2532-2541.
7. Lundqvist, M.; Stigler, J.; Elia, G.; Lynch, I.; Cedervall, T.; Dawson, K. A. Nanoparticle Size and Surface Properties Determine the Protein Corona with Possible Implications for Biological Impacts. *Proc. Natl. Acad. Sci. U.S.A.* **2008,** *105*, 14265.
8. Corbo, C.; Molinaro, R.; Parodi, A.; Toledano Furman, N. E.; Salvatore, F.; Tasciotti, E. The Impact of Nanoparticle Protein Corona on Cytotoxicity, Immunotoxicity and Target Drug Delivery. *Nanomedicine* **2015,** *11*, 81-100.
9. Johnston, B. D.; Kreyling, W. G.; Pfeiffer, C.; Schäffler, M.; Sarioglu, H.; Ristig, S.; Hirn, S.; Haberl, N.; Thalhammer, S.; Hauck, S. M., et al. Colloidal Stability and Surface Chemistry Are Key Factors for the Composition of the Protein Corona of Inorganic Gold Nanoparticles. *Adv. Funct. Mater.* **2017,** *27*, 1701956.
10. Debayle, M.; Balloul, E.; Dembele, F.; Xu, X.; Hanafi, M.; Ribot, F.; Monzel, C.; Coppey, M.; Fragola, A.; Dahan, M., et al. Zwitterionic Polymer Ligands: An Ideal Surface Coating to Totally Suppress Protein-Nanoparticle Corona Formation? *Biomaterials* **2019,** *219*, 119357.
11. Corbo, C.; Mahmoudi, M.; Farokhzad, O. C. Abstract 4642: Personalized Cancer-Specific Protein Corona Affects the Therapeutic Impact of Nanoparticles. *Cancer Res.* **2018,** *78*, 4642.
12. Chen, F.; Wang, G.; Griffin, J. I.; Brenneman, B.; Banda, N. K.; Holers, V. M.; Backos, D. S.; Wu, L.; Moghimi, S. M.; Simberg, D. Complement Proteins Bind to Nanoparticle Protein Corona and Undergo Dynamic Exchange in Vivo. *Nat. Nanotechnol.* **2016,** *12*, 387.
13. Ritz, S.; Schöttler, S.; Kotman, N.; Baier, G.; Musyanovych, A.; Kuharev, J.; Landfester, K.; Schild, H.; Jahn, O.; Tenzer, S., et al. Protein Corona of Nanoparticles: Distinct Proteins Regulate the Cellular Uptake. *Biomacromolecules* **2015,** *16*, 1311-1321.

14. Allen, C.; Qiu, T. A.; Pramanik, S.; Buchman, J. T.; Krause, M. O. P.; Murphy, C. J. Research Highlights: Investigating the Role of Nanoparticle Surface Charge in Nano–Bio Interactions. *Environ. Sci.: Nano* **2017,** *4*, 741-746.
15. Kihara, S.; van der Heijden, N. J.; Seal, C. K.; Mata, J. P.; Whitten, A. E.; Köper, I.; McGillivray, D. J. Soft and Hard Interactions between Polystyrene Nanoplastics and Human Serum Albumin Protein Corona. *Bioconjugate Chem.* **2019,** *30*, 1067-1076.
16. Tavanti, F.; Pedone, A.; Menziani, M. C. Competitive Binding of Proteins to Gold Nanoparticles Disclosed by Molecular Dynamics Simulations. *J. Phys. Chem. C* **2015,** *119*, 22172-22180.
17. Brancolini, G.; Corazza, A.; Vuano, M.; Fogolari, F.; Mimmi, M. C.; Bellotti, V.; Stoppini, M.; Corni, S.; Esposito, G. Probing the Influence of Citrate-Capped Gold Nanoparticles on an Amyloidogenic Protein. *ACS Nano* **2015,** *9*, 2600-2613.
18. Shao, Q.; Hall, C. K. Binding Preferences of Amino Acids for Gold Nanoparticles: A Molecular Simulation Study. *Langmuir* **2016,** *32*, 7888-96.
19. Tavanti, F.; Pedone, A.; Menziani, M. C. A Closer Look into the Ubiquitin Corona on Gold Nanoparticles by Computational Studies. *New J. Chem.* **2015,** *39*, 2474-2482.
20. Buchman, J. T.; Rahnamoun, A.; Landy, K. M.; Zhang, X.; Vartanian, A. M.; Jacob, L. M.; Murphy, C. J.; Hernandez, R.; Haynes, C. L. Using an Environmentally-Relevant Panel of Gram-Negative Bacteria to Assess the Toxicity of Polyallylamine Hydrochloride-Wrapped Gold Nanoparticles. *Environ. Sci.: Nano* **2018,** *5*, 279-288.
21. Qiu, T. A.; Bozich, J. S.; Lohse, S. E.; Vartanian, A. M.; Jacob, L. M.; Meyer, B. M.; Gunsolus, I. L.; Niemuth, N. J.; Murphy, C. J.; Haynes, C. L., et al. Gene Expression as an Indicator of the Molecular Response and Toxicity in the Bacterium *Shewanella Oneidensis* and the Water Flea *Daphnia Magna* Exposed to Functionalized Gold Nanoparticles. *Environ. Sci.: Nano* **2015,** *2*, 615-629.
22. Feng, Z. V.; Gunsolus, I. L.; Qiu, T. A.; Hurley, K. R.; Nyberg, L. H.; Frew, H.; Johnson, K. P.; Vartanian, A. M.; Jacob, L. M.; Lohse, S. E., et al. Impacts of Gold Nanoparticle Charge and Ligand Type on Surface Binding and Toxicity to Gram-Negative and Gram-Positive Bacteria. *Chem. Sci.* **2015,** *6*, 5186-5196.
23. Jacobson, K. H.; Gunsolus, I. L.; Kuech, T. R.; Troiano, J. M.; Melby, E. S.; Lohse, S. E.; Hu, D.; Chrisler, W. B.; Murphy, C. J.; Orr, G., et al. Lipopolysaccharide Density and Structure Govern the Extent and Distance of Nanoparticle Interaction with Actual and Model Bacterial Outer Membranes. *Environ. Sci. Technol.* **2015,** *49*, 10642-10650.
24. Mensch, A. C.; Hernandez, R. T.; Kuether, J. E.; Torelli, M. D.; Feng, Z. V.; Hamers, R. J.; Pedersen, J. A. Natural Organic Matter Concentration Impacts the Interaction of Functionalized Diamond Nanoparticles with Model and Actual Bacterial Membranes. *Environ. Sci. Technol.* **2017,** *51*, 11075-11084.
25. Dominguez, G. A.; Lohse, S. E.; Torelli, M. D.; Murphy, C. J.; Hamers, R. J.; Orr, G.; Klaper, R. D. Effects of Charge and Surface Ligand Properties of Nanoparticles on Oxidative Stress and Gene Expression within the Gut of *Daphnia Magna*. *Aquat. Toxicol.* **2015,** *162*, 1-9.
26. Bozich, J. S.; Lohse, S. E.; Torelli, M. D.; Murphy, C. J.; Hamers, R. J.; Klaper, R. D. Surface Chemistry, Charge and Ligand Type Impact the Toxicity of Gold Nanoparticles to Daphnia Magna. *Environ. Sci.: Nano* **2014,** *1*, 260-270.
27. Melby, E. S.; Lohse, S. E.; Park, J. E.; Vartanian, A. M.; Putans, R. A.; Abbott, H. B.; Hamers, R. J.; Murphy, C. J.; Pedersen, J. A. Cascading Effects of Nanoparticle Coatings: Surface

Functionalization Dictates the Assemblage of Complexed Proteins and Subsequent Interaction with Model Cell Membranes. *ACS Nano* **2017,** *11*, 5489-5499.
28. Lin, W.; Insley, T.; Tuttle, M. D.; Zhu, L.; Berthold, D. A.; Král, P.; Rienstra, C. M.; Murphy, C. J. Control of Protein Orientation on Gold Nanoparticles. *J. Phys. Chem. C* **2015,** *119*, 21035-21043.
29. Tollefson, E. J.; Allen, C. R.; Chong, G.; Zhang, X.; Rozanov, N. D.; Bautista, A.; Cerda, J. J.; Pedersen, J. A.; Murphy, C. J.; Carlson, E. E., et al. Preferential Binding of Cytochrome C to Anionic Ligand-Coated Gold Nanoparticles: A Complementary Computational and Experimental Approach. *ACS Nano* **2019,** *13*, 6856.
30. Yousefi, N.; Tufenkji, N.; Shao, Q.; Hall, C. K. Probing the Interaction between Nanoparticles and Lipid Membranes by Quartz Crystal Microbalance with Dissipation Monitoring. *Front. Chem.* **2016,** *4*, 46.
31. Melby, E. S.; Allen, C.; Foreman-Ortiz, I. U.; Caudill, E. R.; Kuech, T. R.; Vartanian, A. M.; Zhang, X.; Murphy, C. J.; Hernandez, R.; Pedersen, J. A. Peripheral Membrane Proteins Facilitate Nanoparticle Binding at Lipid Bilayer Interfaces. *Langmuir* **2018,** *34*, 10793-10805.
32. Cederquist, K. B.; Keating, C. D. Curvature Effects in DNA:Au Nanoparticle Conjugates. *ACS Nano* **2009,** *3*, 256-260.
33. Hill, H. D.; Millstone, J. E.; Banholzer, M. J.; Mirkin, C. A. The Role Radius of Curvature Plays in Thiolated Oligonucleotide Loading on Gold Nanoparticles. *ACS Nano* **2009,** *3*, 418-424.
34. Mandal, H. S.; Kraatz, H.-B. Effect of the Surface Curvature on the Secondary Structure of Peptides Adsorbed on Nanoparticles. *J. Am. Chem. Soc.* **2007,** *129*, 6356-6357.
35. Villarreal, E.; Li, G. G.; Zhang, Q.; Fu, X.; Wang, H. Nanoscale Surface Curvature Effects on Ligand–Nanoparticle Interactions: A Plasmon-Enhanced Spectroscopic Study of Thiolated Ligand Adsorption, Desorption, and Exchange on Gold Nanoparticles. *Nano Lett.* **2017,** *17*, 4443-4452.
36. Phillips, J. C.; Braun, R.; Wang, W.; Gumbart, J.; Tajkhorshid, E.; Villa, E.; Chipot, C.; Skeel, R. D.; Kalé, L.; Schulten, K. Scalable Molecular Dynamics with Namd. *J. Comput. Chem.* **2005,** *26*, 1781-802.
37. Brooks, B. R.; Brooks III, C. L.; Mackerell Jr, A. D.; Nilsson, L.; Petrella, R. J.; Roux, B.; Won, Y.; Archontis, G.; Bartels, C.; Boresch, S. Charmm: The Biomolecular Simulation Program. *J. Comput. Chem.* **2009,** *30*, 1545-1614.
38. Martínez, L.; Andrade, R.; Birgin, E. G.; Martínez, J. M. Packmol: A Package for Building Initial Configurations for Molecular Dynamics Simulations. *J. Comput. Chem.* **2009,** *30*, 2157-2164.
39. Torelli, M. D.; Putans, R. A.; Tan, Y.; Lohse, S. E.; Murphy, C. J.; Hamers, R. J. Quantitative Determination of Ligand Densities on Nanomaterials by X-Ray Photoelectron Spectroscopy. *ACS Appl. Mater. Inter.* **2015,** *7*, 1720-1725.
40. Humphrey, W.; Dalke, A.; Schulten, K. {Vmd}: Visual Molecular Dynamics. *J. Mol. Graph.* **1996,** *14*, 33-8, 27-8.
41. Price, D. J.; Brooks, C. L. A Modified Tip3p Water Potential for Simulation with Ewald Summation. *J. Chem. Phys.* **2004,** *121*, 10096-103.
42. Plimpton, S. Fast Parallel Algorithms for Short-Range Molecular Dynamics. *J. Comput. Phys.* **1995,** *117*, 1-19.

43. Ghorai, P. K.; Glotzer, S. C. Molecular Dynamics Simulation Study of Self-Assembled Monolayers of Alkanethiol Surfactants on Spherical Gold Nanoparticles. *J. Phys. Chem. C* **2007,** *111*, 15857-15862.
44. Banci, L.; Bertini, I.; Gray, H. B.; Luchinat, C.; Reddig, T.; Rosato, A.; Turano, P. Solution Structure of Oxidized Horse Heart Cytochrome C. *Biochemistry* **1997,** *36*, 9867-9877.
45. Tuominen, E. K. J.; Wallace, C. J. A.; Kinnunen, P. K. J. Phospholipid-Cytochrome C Interaction: Evidence for the Extended Liipid Anchorage. *J. Biol. Chem.* **2002,** *277*, 8822-8826.
46. Kinnunen, P. K. J.; Kõiv, A.; Lehtonen, J. Y. A.; Rytömaa, M.; Mustonen, P. Lipid Dynamics and Peripheral Interactions of Proteins with Membrane Surfaces. *Chem. Phys. Lipids* **1994,** *73*, 181-207.
47. Rytömaa, M.; Kinnunen, P. K. Evidence for Two Distinct Acidic Phospholipid-Binding Sites in Cytochrome C. *J. Biol. Chem.* **1994,** *269*, 1770-1774.
48. Neidhart, S. M.; Gezelter, J. D. Thermal Transport Is Influenced by Nanoparticle Morphology: A Molecular Dynamics Study. *J. Phys. Chem. C* **2018,** *122*, 1430-1436.
49. Walt, S. v. d.; Colbert, S. C.; Varoquaux, G. The Numpy Array: A Structure for Efficient Numerical Computation. *Comput. Sci. Eng.* **2011,** *13*, 22-30.
50. Kluyver, T.; Ragan-Kelley, B.; Pérez, F.; Granger, B.; Bussonnier, M.; Frederic, J.; Kelley, K.; Hamrick, J.; Grout, J.; Corlay, S., et al. In *Jupyter Notebooks -- a Publishing Format for Reproducible Computational Workflows*, 2016; Loizides, F.; Schmidt, B., Eds. pp 87-90.
51. Pale-Grosdemange, C.; Simon, E. S.; Prime, K. L.; Whitesides, G. M. Formation of Self-Assembled Monolayers by Chemisorption of Derivatives of Oligo(Ethylene Glycol) of Structure Hs(Ch2)11(Och2ch2)Moh on Gold. *J. Am. Chem. Soc.* **1991,** *113*, 12-20.
52. Brust, M.; Walker, M.; Bethell, D.; Schiffrin, D. J.; Whyman, R. Synthesis of Thiol-Derivatised Gold Nanoparticles in a Two-Phase Liquid–Liquid System. *J. Chem. Soc., Chem. Commun.* **1994**, 801-802.
53. Li, Y.; Zaluzhna, O.; Zangmeister, C. D.; Allison, T. C.; Tong, Y. J. Different Mechanisms Govern the Two-Phase Brust–Schiffrin Dialkylditelluride Syntheses of Ag and Au Nanoparticles. *J. Am. Chem. Soc.* **2012,** *134*, 1990-1992.
54. Sweeney, S. F.; Woehrle, G. H.; Hutchison, J. E. Rapid Purification and Size Separation of Gold Nanoparticles Via Diafiltration. *J. Am. Chem. Soc.* **2006,** *128*, 3190-3197.
55. Rodahl, M.; Höök, F.; Krozer, A.; Brzezinski, P.; Kasemo, B. Quartz Crystal Microbalance Setup for Frequency and Q ‐ Factor Measurements in Gaseous and Liquid Environments. *Rev. Sci. Instrum.* **1995,** *66*, 3924-3930.
56. Wu, M.; Vartanian, A. M.; Chong, G.; Pandiakumar, A. K.; Hamers, R. J.; Hernandez, R.; Murphy, C. J. Solution Nmr Analysis of Ligand Environment in Quaternary Ammonium-Terminated Self-Assembled Monolayers on Gold Nanoparticles: The Effect of Surface Curvature and Ligand Structure. *J. Am. Chem. Soc.* **2019,** *141*, 4316-4327.
57. Lin, J.; Zhang, H.; Morovati, V.; Dargazany, R. Pegylation on Mixed Monolayer Gold Nanoparticles: Effect of Grafting Density, Chain Length, and Surface Curvature. *J. Colloid Interface Sci.* **2017,** *504*, 325-333.
58. Kataoka, M.; Hagihara, Y.; Mihara, K. i.; Goto, Y. Molten Globule of Cytochrome C Studied by Small Angle X-Ray Scattering. *J. Mol. Biol.* **1993,** *229*, 591-596.

59. Garcia-Fuentes, M.; Torres, D.; Martín-Pastor, M.; Alonso, M. J. Application of Nmr Spectroscopy to the Characterization of Peg-Stabilized Lipid Nanoparticles. *Langmuir* **2004,** *20*, 8839-8845.
60. Thevenot, J.; Troutier, A.-L.; David, L.; Delair, T.; Ladavière, C. Steric Stabilization of Lipid/Polymer Particle Assemblies by Poly(Ethylene Glycol)-Lipids. *Biomacromolecules* **2007,** *8*, 3651.
61. Tuominen, E. K. J.; Wallace, C. J. A.; Kinnunen, P. K. J. Phospholipid-Cytochrome C Interaction: Evidence for the Extended Lipid Anchorage. *J. Biol. Chem.* **2002,** *277*, 8822-8826.
62. Hannibal, L.; Tomasina, F.; Capdevila, D. A.; Demicheli, V.; Tórtora, V.; Alvarez-Paggi, D.; Jemmerson, R.; Murgida, D. H.; Radi, R. Alternative Conformations of Cytochrome C: Structure, Function, and Detection. *Biochemistry* **2016,** *55*, 407-428.

Table of Content Graphic

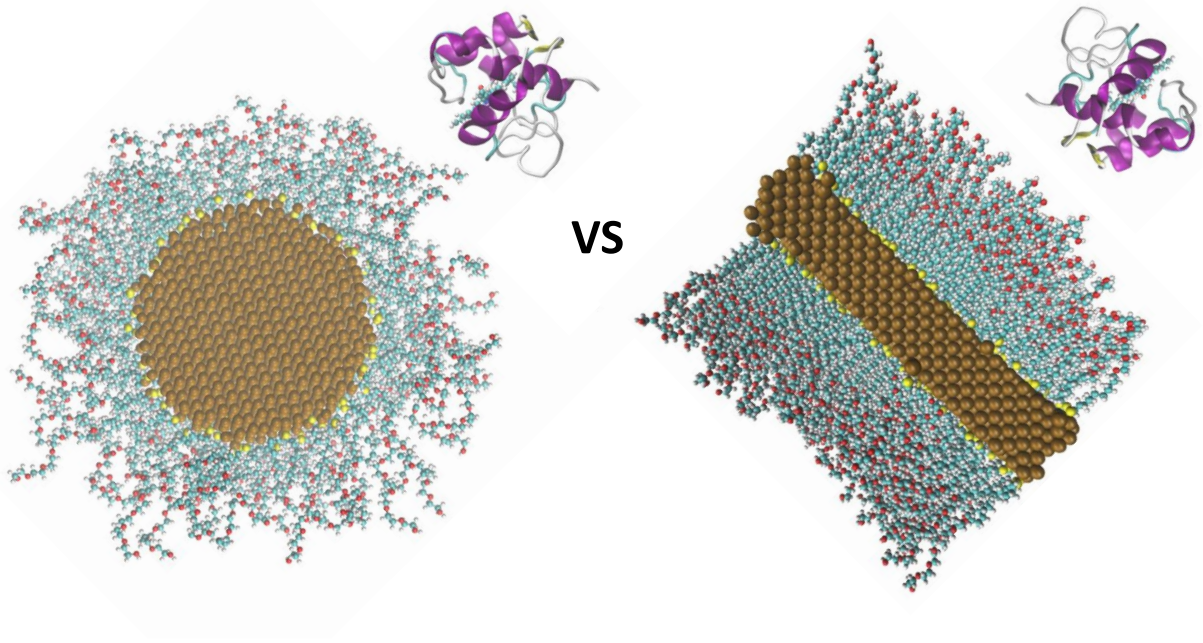

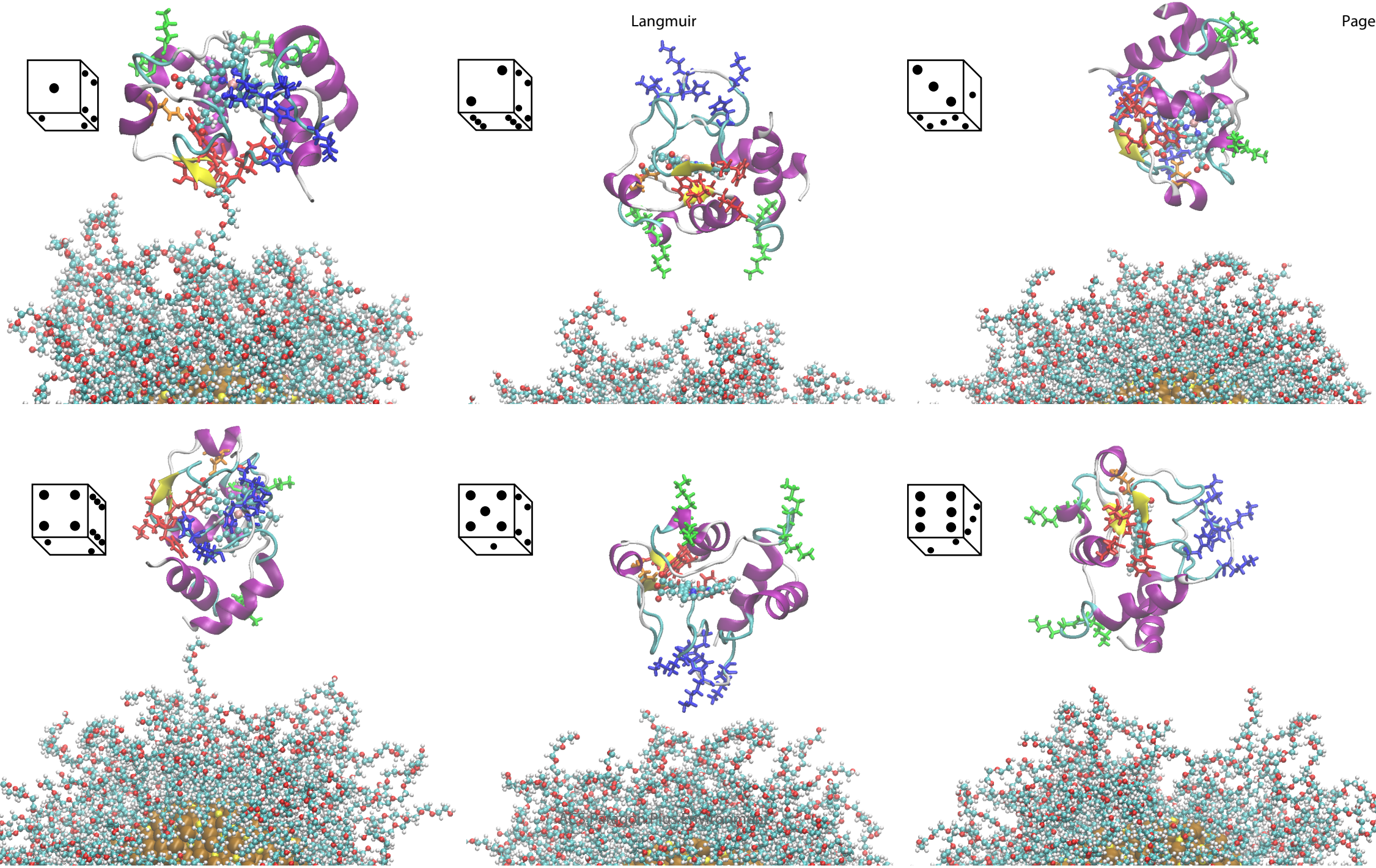

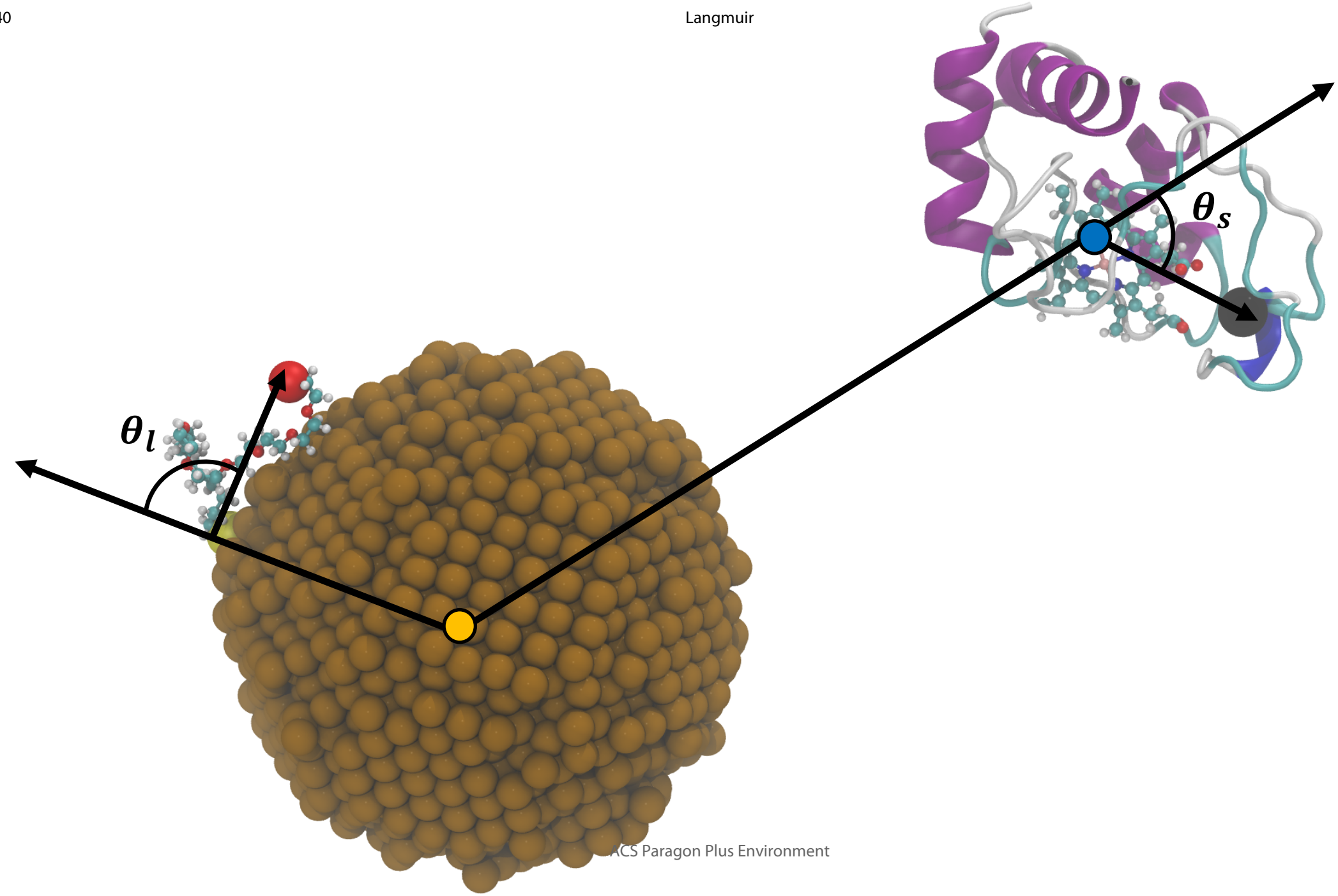
θ_l
θ_s

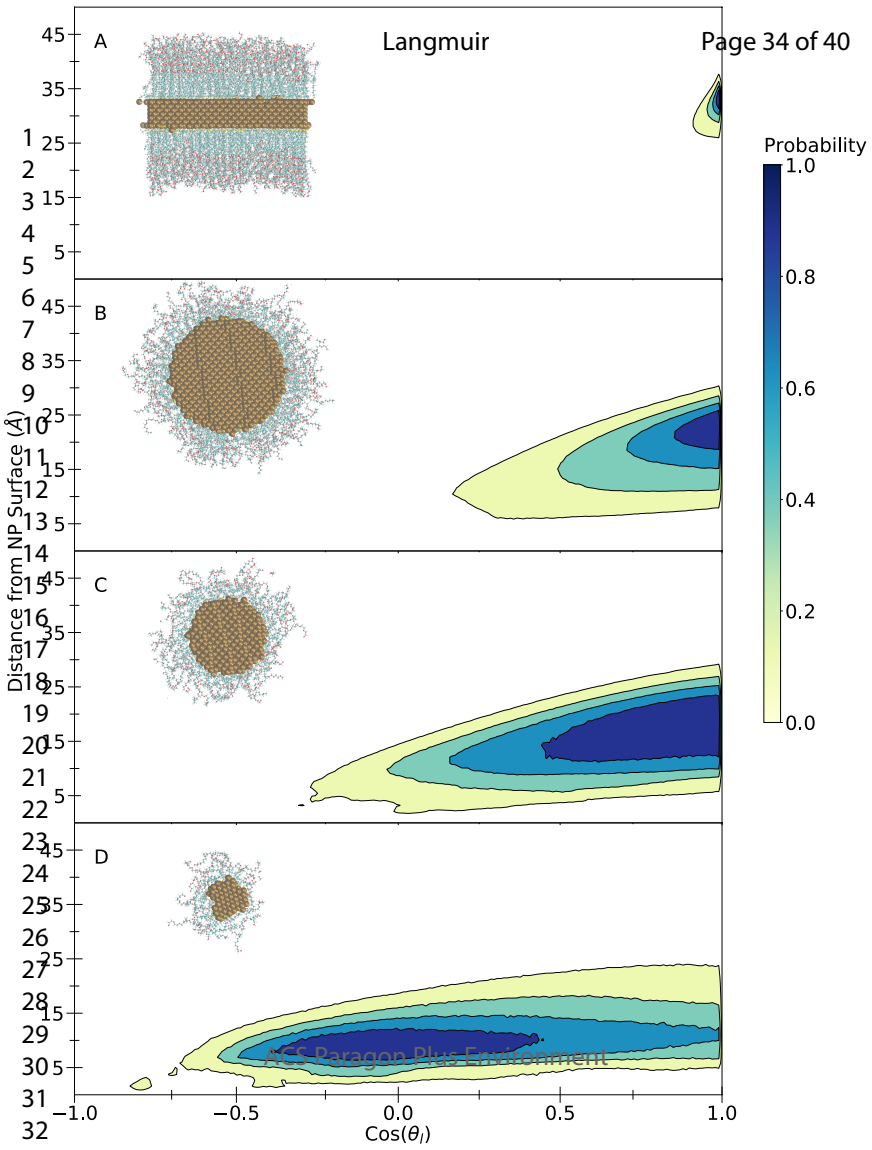

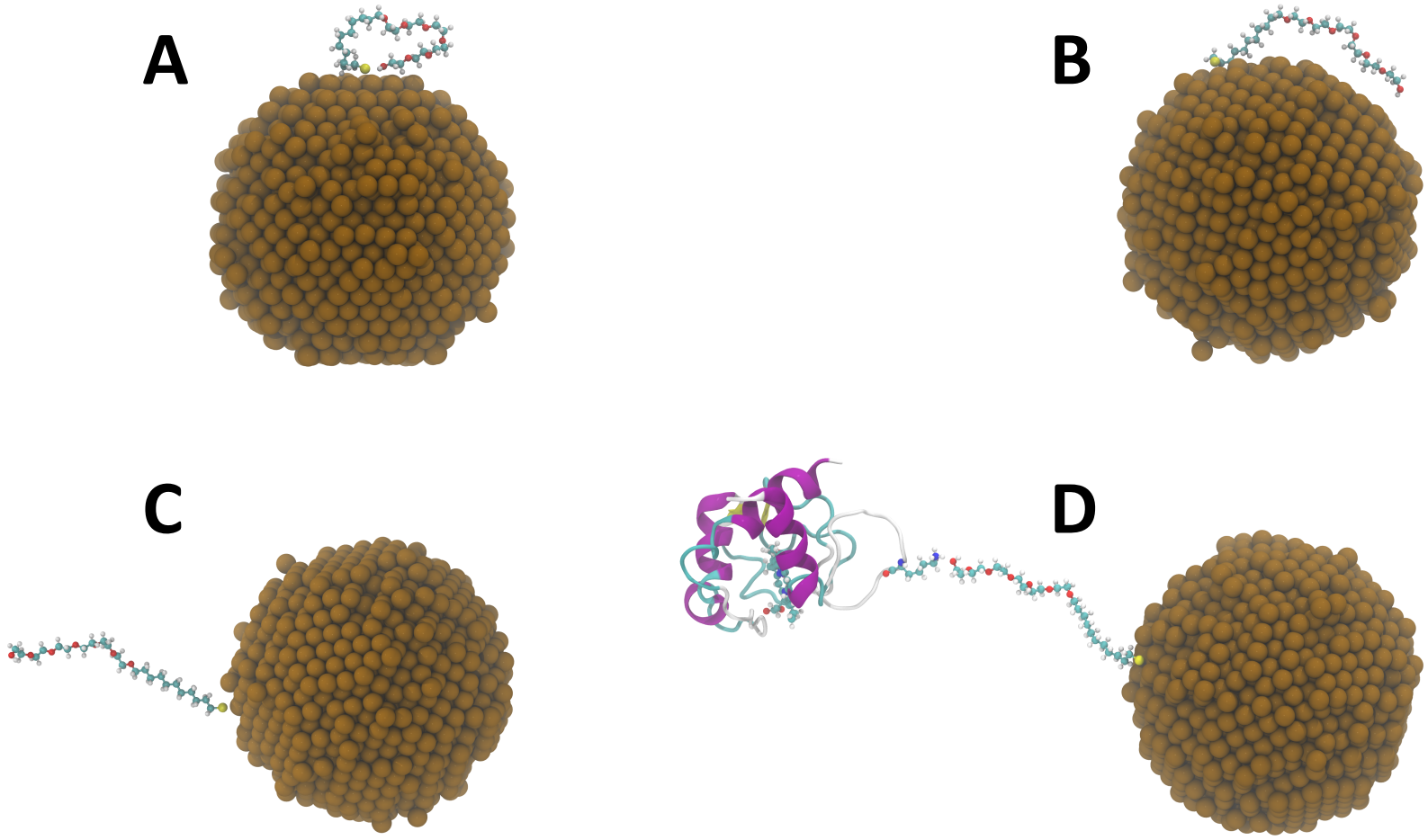
A
B
C
D

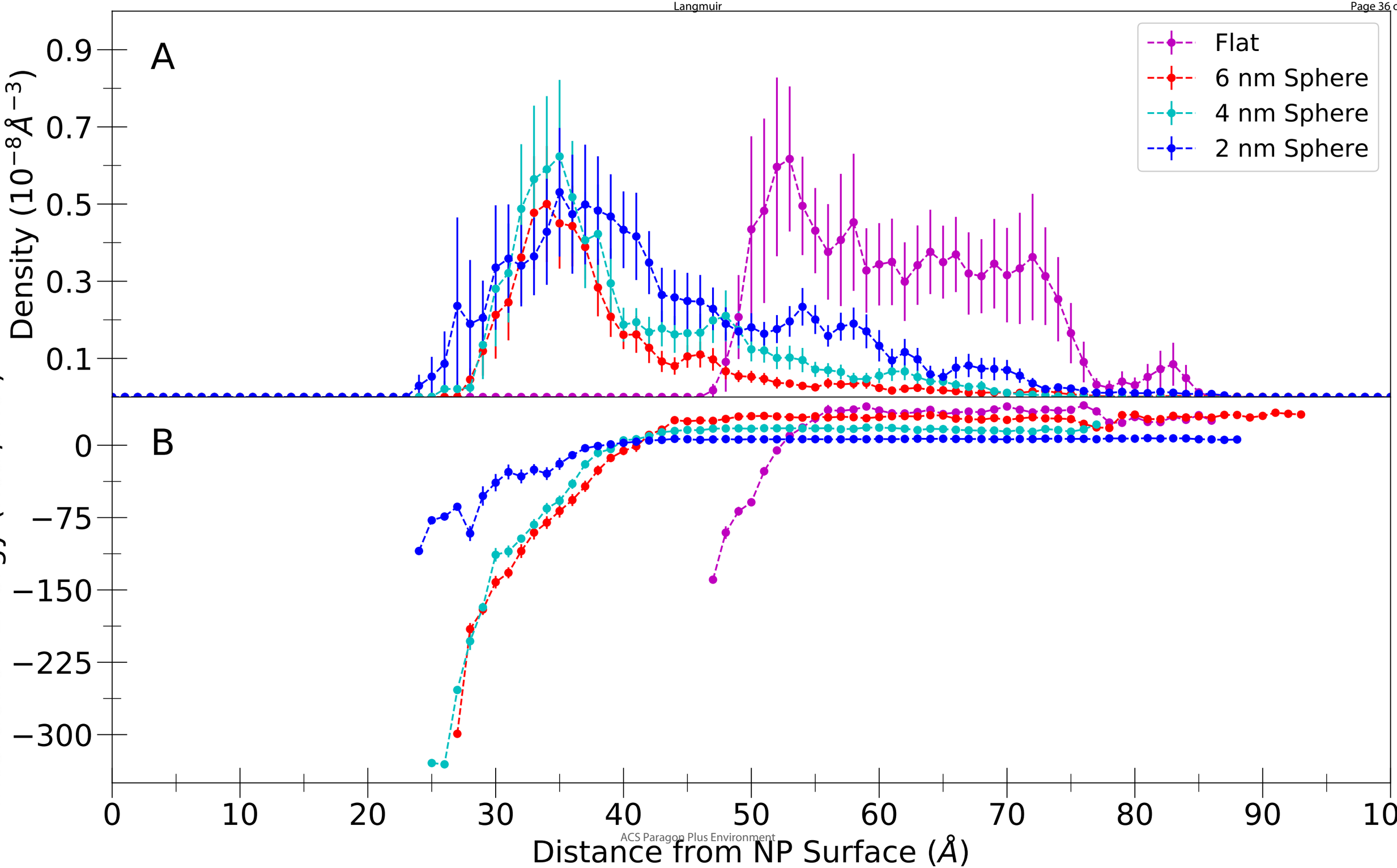
A
B
Flat
6 nm Sphere
4 nm Sphere
2 nm Sphere
Density ($10^{-8}Å^{-3}$)
Interaction Energy (kcal/mol)
Distance from NP Surface ($Å$)
0.9
0.7
0.5
0.3
0.1
0
−75
−150
−225
−300
0
10
20
30
40
50
60
70
80
90
100

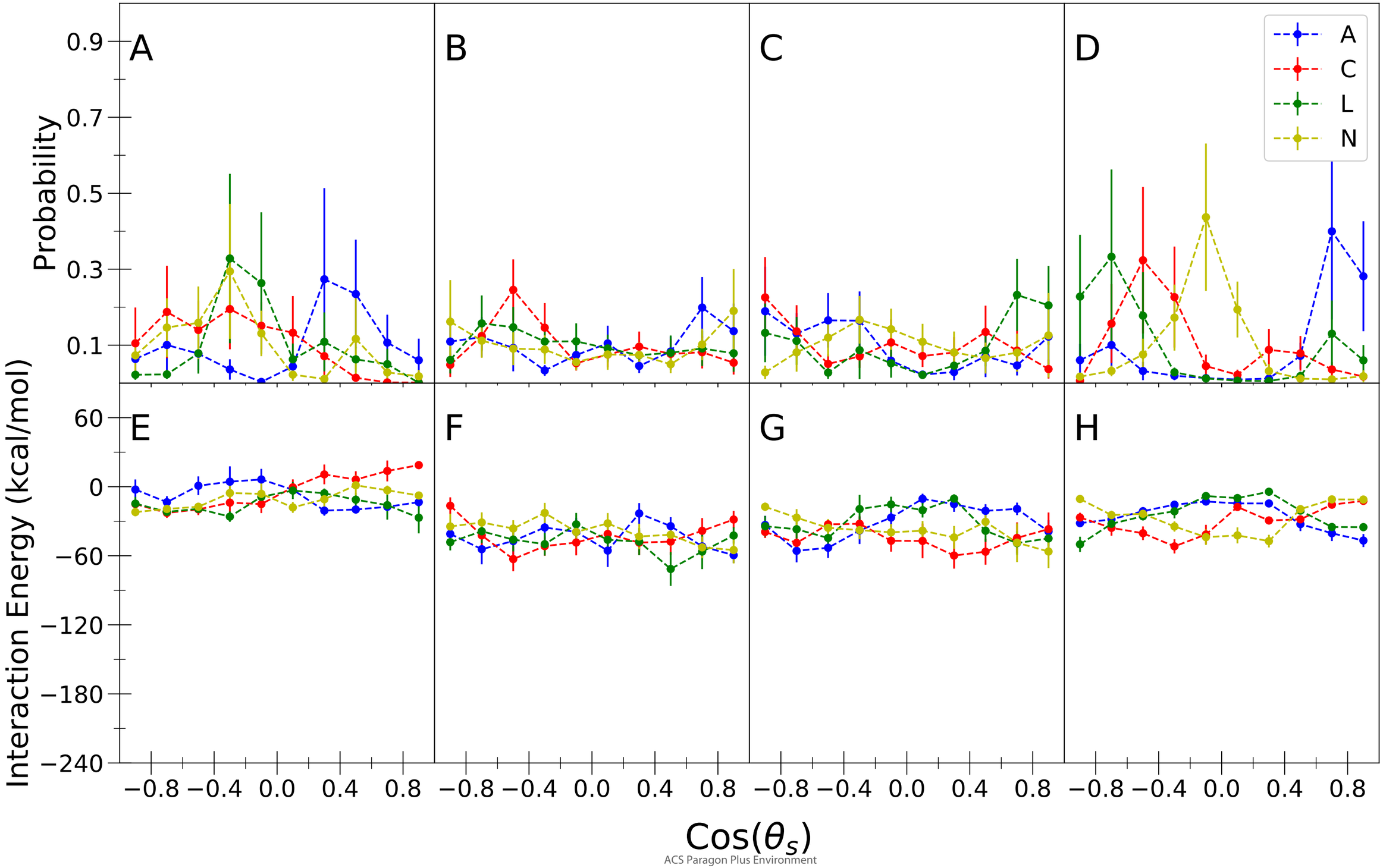
A
B
C
D
E
F
G
H
A
C
L
N
Probability
0.9
0.7
0.5
0.3
0.1
Interaction Energy (kcal/mol)
60
0
−60
−120
−180
−240
−0.8 −0.4 0.0 0.4 0.8
Cos(θs)

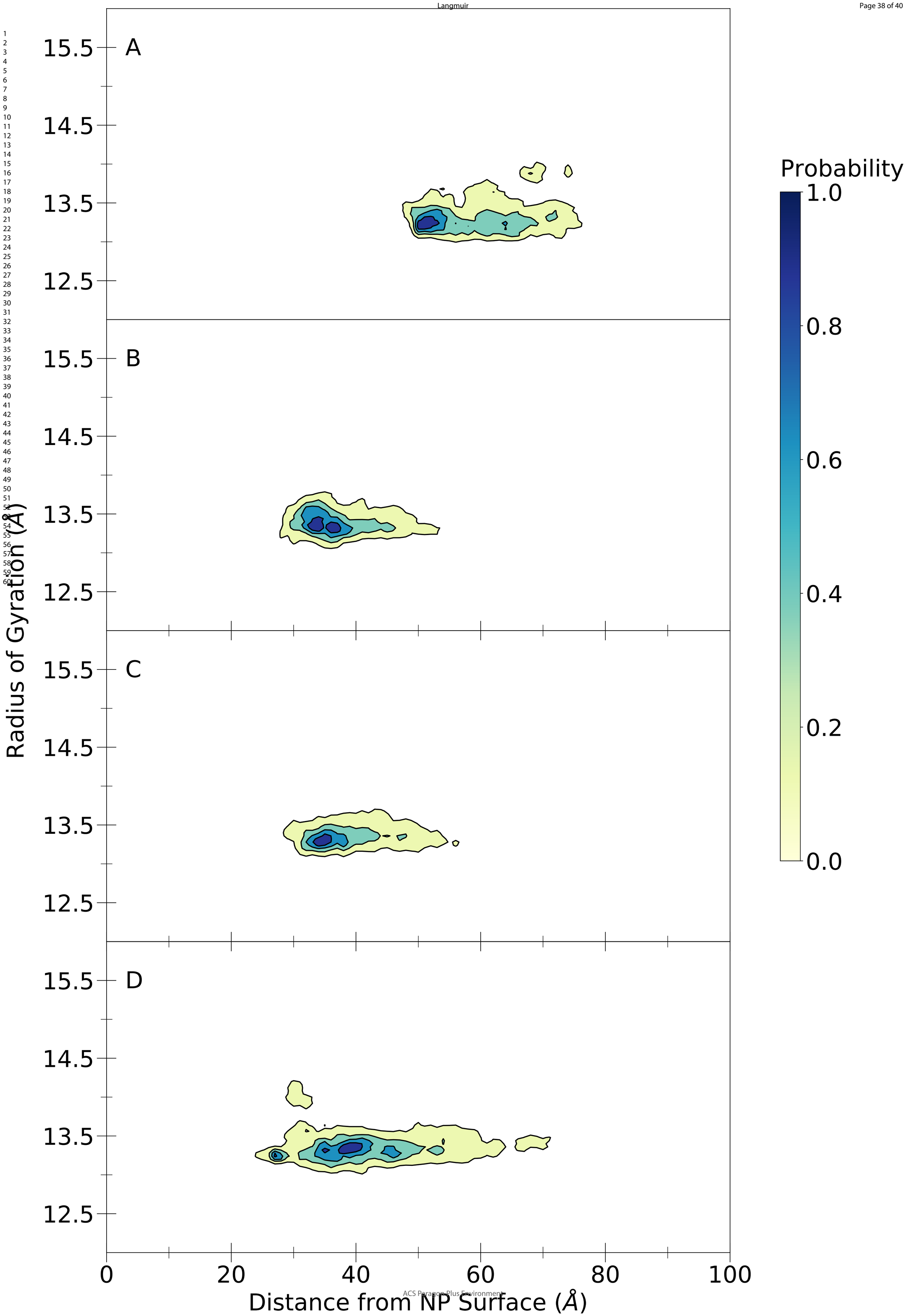
A
B
C
D
15.5
14.5
13.5
12.5
Radius of Gyration (Å)
Distance from NP Surface (Å)
0
20
40
60
80
100
Probability
1.0
0.8
0.6
0.4
0.2
0.0

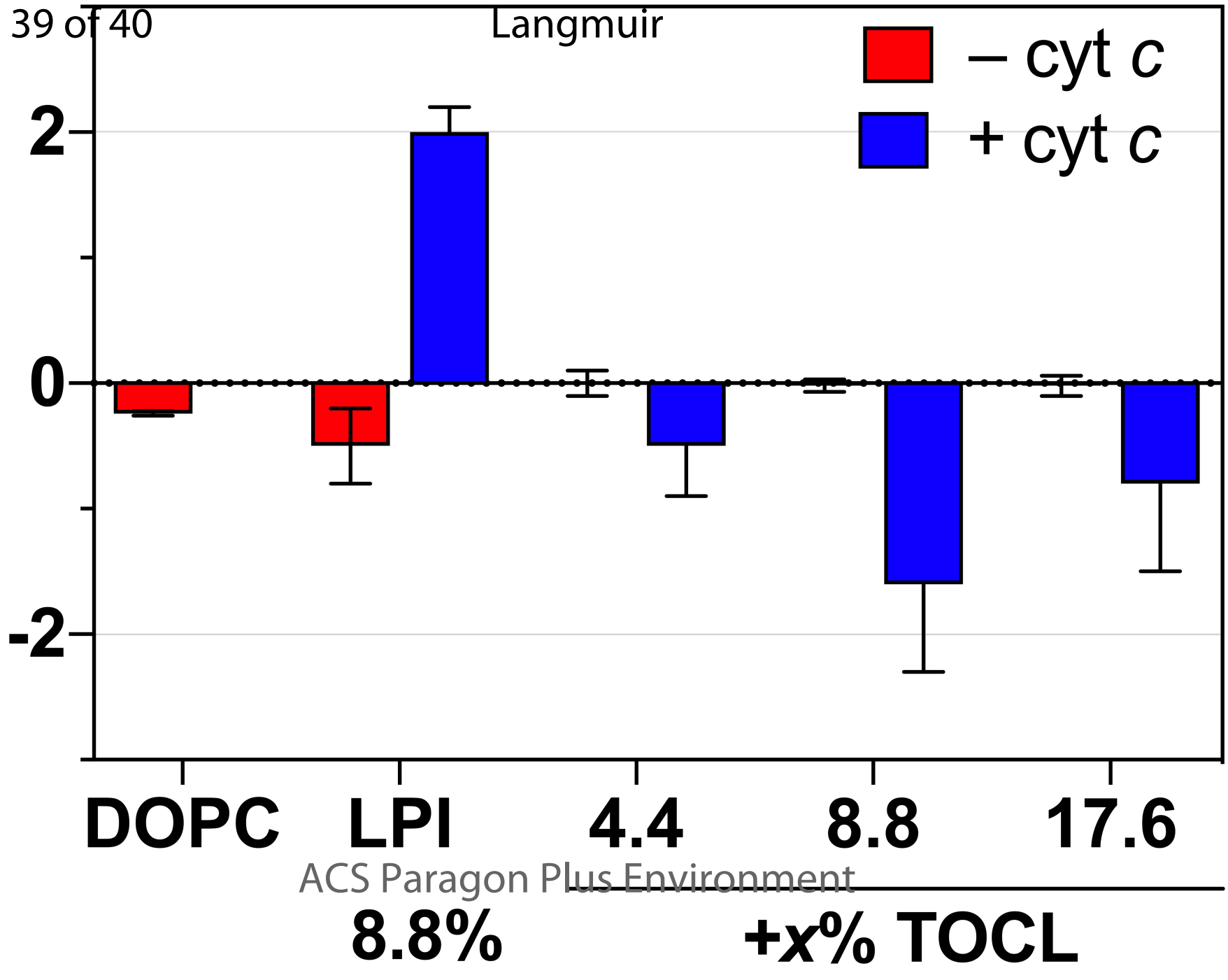

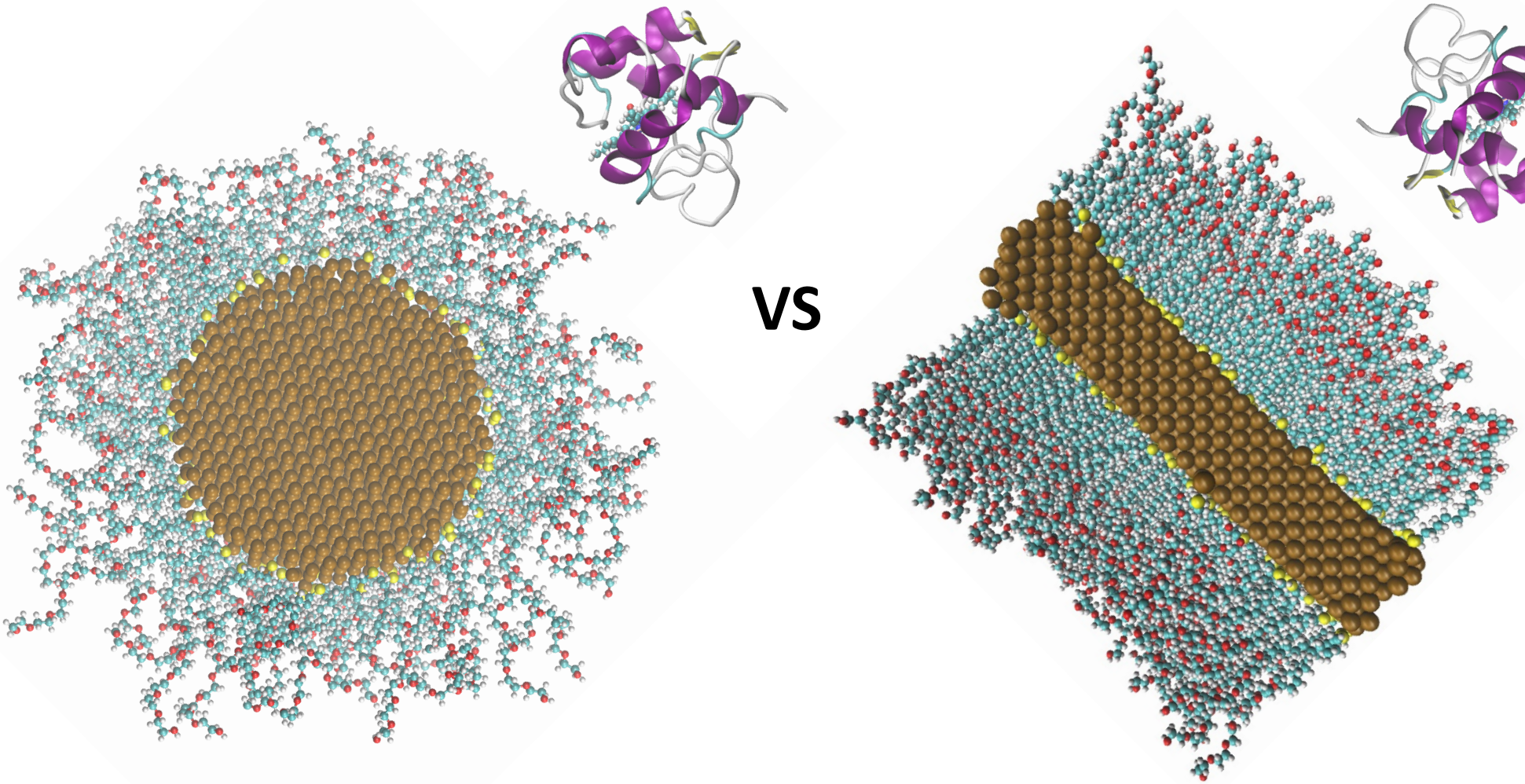
VS